Regression Analysis of Octal Rings as Mechanical Force Transducers

KHALED A. ABUHASEL* & ESSAM SOLIMAN**
*Department of Mechanical Engineering
College of Engineering, University of Bisha, Bisha, Kingdom of Saudi Arabia
**Department of Mechanical Engineering
College of Engineering, Prince Sattam bin Abdulaziz University
Al-kharj, Kingdom of Saudi Arabia
*kabuhasel@hotmail.com & **essam.a.soliman@gmail.com
** On leave, from Department of Production Engineering, Faculty of Engineering, Alexandria University.

Abstract: - This paper presents analytical approach for octal rings as mechanical force transducers. The work first analyzes the characteristics of octal rings as mechanical force transducers, using a finite element model of the ring to determine its state of strain upon the application of load. It also correlates correlate ring design parameters and performance measures using an L9 orthogonal array of finite element simulations. Design parameters include height, thickness, width, and edge curvature. Performance measures include sensitivity and stiffness. Model simulation results showed considerable variation in strain along ring face with considerable difference in maximum values between tensile and compressive strains. Also, revealed a region of a relatively large tensile strain within the ring not addressed in the literature. The relation between strain gauge length and average strain revealed an optimal gauge length that improves ring performance. Moreover, simulation results showed that increasing ring height and decreasing its thickness increases its sensitivity and decreases its stiffness. Finally, results of the regression analysis indicated that there is enough statistical evidence to say that the parameters, height and thickness, influences the stiffness response and the parameters, height, thickness, and width, influences the sensitivity response.

Key-Words: - Octal rings, strain gauge, average strain, sensitivity, stiffness, force transducer, regression analysis.

1 Introduction

Mechanical force measurement has a wide range of applications. They include weighing systems, material testing, and performance evaluation of equipment. In addition, mechanical force measurement is essential for performance improvement and optimization of machining processes. Tool breakage detection and chatter control depend on the measurement of machining forces, and on line analysis of force signals. In addition, prediction of chip loading and accuracy of machined surface rely on force measurement.

A considerable amount of research work focused on analyzing performance characteristics of octal rings. The purpose was to use them as force sensors for constructing force dynamometers. M. Korencke and M.L. Hull [1] developed empirical formulae to describe strain, stress and deflection in octagonal rings. They used ANSYS finite element model and a nonlinear regression model to develop the equations. There was reasonable agreement between experimental data and model equations. The developed equations provided close results to experimental data compared to equations available from thin ring theory. However, validity of equations was limited to range of ring thickness and width.

Jeong-Du Kim and Dang-Sik Kim [2] developed a combined type tool dynamometer for an ultra-precise lathe. They used strain gauges to measure static force and a piezo-electric film accelerator to measure dynamic force. They pointed out that signal conditioning and processing are essential for improving accuracy of force measurement.

Ulvi Seker et al [3] used a bending beam type dynamometer the main to measure machining force for the shaping process. Even though the authors designed the dynamometer, they did not give enough details of its construction. They gave the general characteristics of the load cell used. They focused of the measured force data rather than on the design of dynamometer. They used cutting force data to correlate cutting parameters including depth of cut and federate to process performance measures

including surface roughness of work part and tool life.

Ihsan Korkotand Sedat Karabay [4, 5] used octal strain rings to design milling and drilling dynamometers. They used approximate equations to estimate strain and stiffness in octal rings. They claimed that the dynamometers could measure cutting force with ±5 N sensitivity and 0.05% or less cross sensitively. They presented no information regarding strain gauge type or dimensions. In addition, they did not show clearly the procedure for recording and processing signals from dynamometer.

SuleymanYaldiz, and FarukUnsacar [6,7] designed a three-components force dynamometers for the measurement of cutting force in turning. They, also, used octal rings as sensing element and used approximate equations from thin ring theory to design the rings. The range of the measured force was 3500N. Sensitivity was ±5 N and cross sensitivity was 0.17-0.92%. Length of strain gauge was 6 mm, about 30% of the length of the octal ring face, which was 16.6 mm.

Y. Chen et. al. [8] used extended octal rings and strain gauges to design a dynamometer for a tractor drawbar. They used finite element analysis to determine points of maximum strain at the rings. They fixed strain gauges at these points to get maximum possible sensitively of the dynamometer. However, they did not consider strain distribution around points of maximum strain.

Sadat Karabay [9, 10, and 11] used strain gauges with different forms of octal strain rings to design force dynamometers for the drilling and milling processes. They used equations from thin ring theory for the design of the rings. No attention was given to strain distribution along the area where strain gauges were fixed. They used calibration to correlate signal from a strain gauge bridge and cutting forces.

Suleyman Yalidz et. al. [12] used octal rings and strain gauges to design a force dynamometer for the milling process. They determined the dynamic characteristics of the dynamometer using the impact test. They showed that the natural frequencies of the dynamometers were low. The only extra feature in their design is using large number of strain gauges to increase dynamometer sensitively.

This work considers octal rings as sensing element for measuring mechanical force, together with strain gauges. The aim of the work is to investigate strain distribution along the different faces and regions of the ring, with the purpose of deciding on the best area on the ring to adhere strain gauges to end up with maximum possible sensitivity to mechanical force.

In addition, this work, considers the correlation between design parameters of the ring and its performance measures.

Mechanical forces are measured indirectly using two main techniques; in the first one, the force acts on a piezoelectric crystal that accumulates charge proportional to the magnitude of the force. A charge amplifier, then, converts charges to volt. In general, piezoelectric sensors are very sensitive to mechanical forces and have wide bandwidth, over 50 KHz. They are available in different configurations and sensitivities. In addition, charge amplifiers are available in wide range of configuration and characteristics. However, they are expensive, delicate and require a considerable attention when used within the harsh machining environment. They are susceptible to noise from nearby electrical drives. Therefore, the present work will not consider piezoelectric sensors.

In the second technique, the force acts on an elastic mechanical member. The strain and deflection of the member are proportional to force. A common mechanical member for force measurement is octal ring. A strain gauge converts strain in the strain ring into equivalent volt using a bridge. Octal rings are easy to manufacture to the required size. Strain gauges are relatively inexpensive and are available in a wide range of configurations and characteristics. In addition, bridges, in particular Wheatstone bridge, are easy to operate and maintain. Therefore, octal rings with strain gauges are the candidate for sensing mechanical forces in the present work.

2 Geometric Models

In order to study the state of strain of octal rings, a 3D geometrical model of a ring was constructed using the Solid Edge Software package. Fig. 1 shows the model. The basic design parameters are height, H, width, W, thickness, T, and edge radius R. Other parameters such as face length, L_s and inner hole diameter, D, are derived from the basic design parameters. Then, the finite element method was applied to the model using the same software package.

Tetrahedral finite elements were used for the finite element model as shown in Fig. 1. The material of the ring was selected to be Aluminum 1060 with 68.947 GPa modulus of elasticity, 0.33 Poisson ratio, 27.579 MPa yield stress and 68.948 MPa ultimate tensile strength. Fig 1, also, shows faces and regions of interest where maximum strains

or maximum deformations are expected to take place.

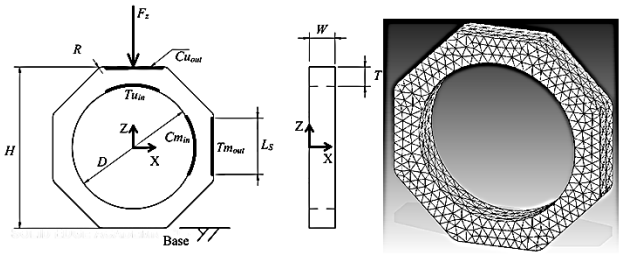

Fig. 1 Geometric and finite element models and basic design parameters of the octal ring.

A concentrated force, F_z, is applied normal to the face Cu_{out}, in the negative z-direction. The concentrated force represents the worst loading condition of the ring considering deflection and ring stiffness. The magnitude of the force is selected to be $F_z = 100$ N. Such selection ensures no plastic deformation takes place within the ring for the range of design parameters used for the present work and given in the next section. The model considers a ring rigidly fixed at its bottom surface. This simulates a ring welded to its base. The method of fixation of the ring affects mainly state of strain and stress around the fixation region. However, interest is in strains at faces and regions away from ring bottom. Therefore, this work does not give the method of fixation a considerable attention. In addition, the applied force tends to fix the bottom face of the ring to its base. Upon application of the load and simulating the model, stresses and strains of all surface finite elements of the ring were available. Strains at the elements within the aforementioned faces and regions of interest were recorded manually using a strain pick feature of the software. In addition, the positions of the elements, with respect of the XYZ coordinate system of Fig. 1, were recorded and stored in data structures within the MATLAB software. All strains, deformations and stresses, were recorded in the ZX-plane.

3 Design of simulations

Performance measures of an octal ring are mainly sensitivity and stiffness. Sensitivity, S_z, is defined as:

$$S_z = \frac{\varepsilon^{max}}{F_z} \qquad (1)$$

Where F_z is the force acting on the ring and ε_{max} is the maximum measurable strain in the ring.

Similarly, stiffness, K_z, of the ring is defined as:

$$K_z = \frac{F_z}{\alpha^{max}} \qquad (2)$$

Where, α_{max} is the maximum measurable deflection at the Cu_{out} surface of the ring, basically, at the point of application of the load.

The suffix z in equations 1 and 2 indicates that sensitivity and stiffness are determined in the z-direction. Sensitivity and stiffness of the ring in the x-direction can be dealt with in the same way as in z-direction and, therefore, are not considered in the present work.

Finite element simulations were conducted to correlate the design parameters and the performance measures. Simulation design parameters followed an L_9 orthogonal array. Table 1 shows the levels of design parameters for the simulations. The table also gives the values of the derived parameters.

Because the size of the ring varies from one simulation to another, the number of finite elements, N_f, and number of nodes, N_n, for the finite element model vary as well. Finite element size, E_s, is selected to give reasonably smooth strain distribution. Table 1 gives values of finite element model parameters.

Table 1 Levels of design parameters

SIM	Design parameters				Derived parameters		Finite element simulation		
	H [mm]	T [mm]	W [mm]	R [mm]	L_s [mm]	D [mm]	N_f	N_n	E_s [mm]
1	50	4	6	0	20.71	42	66094	100153	0.37
2	50	6	8	2	19.05	38	29845	137987	0.37
3	50	8	10	4	17.40	34	497094	714962	0.22
4	40	4	8	4	13.26	32	89529	133056	0.33
5	40	6	10	0	16.57	28	169484	246681	0.30
6	40	8	6	2	14.91	24	151830	221996	0.29
7	30	4	10	2	10.77	22	495333	708939	0.16
8	30	6	6	4	9.11	18	153450	223804	0.23
9	30	8	8	0	12.43	14	266732	376408	0.37

4 Results and Discussions

Fig 2.a shows strain distribution along the face Tm_{out} for SIM 2. The dashed line represents the ring profile while the solid line represents the strain distribution. The strain, ε_t, is in tension state and therefore, has positive values in the figure. The figure also shows the z-positions of the element of the face at which ε_t is recorded. It can be observed from the figure that the strain varies considerably along the face and the max strain, $\varepsilon_t^{max} = 67.7$ [μm/m], is almost seven times larger than the minimum strain, 10 [μm/m]. Fig. 2.c is an enlarged view of Fig 2.a, around the middle of Tm_{out} where the z-position is zero.

It can be observed from the figure that ε_t^{max} is shifted from the center of the face, Tm_{out} by 1.14 [mm]. The shift value corresponds to 6% of the length of Tm_{out}, L_s. In the literature, [5, 6] ε_t^{max} is usually considered at the middle of Tm_{out}. Fig 2.b shows strain distribution over the region Cm_{in} for the same simulation, SIM 2. Again, the dashed line

represents the ring profile while the solid line represents strain distribution. The strain, ε_c, is in compression state, and is represented by negative values. The figure also gives the z- position of the elements of the region Cm_{in} at which ε_c is recorded. From figure, it can be observed that ε_c^{max} is 100.9 [μm/m] which is 63% larger than ε_t^{max}. Fig. 2.d is also an enlarged view of Fig. 2.b around the zero z-position. It shows that ε_c^{max} is shifted by 0.77 [mm] from the zero z-position. The distributions of ε_t and ε_c and the consequent observations are the same for all simulations. Strain ε_c is always larger, in absolute value, than ε_t. Also, both ε_t^{max} and ε_c^{max} are shifted from the zero z-position by different values. Table 2 summarizes the results of all simulations for ε_t^{max} and ε_c^{max} values and the corresponding shift values. The implication of the aforementioned observations is nonlinear relation between the load and output volt of any force sensor using octal rings as transducers. It is common to give force sensor maximum nonlinearity as a sensor specification. Understanding the source of such nonlinearity helps in reducing it and thus improving sensor performance.

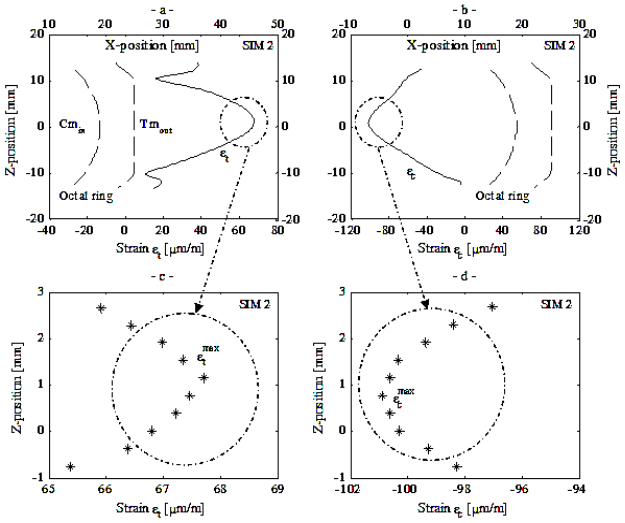

Fig. 2 Strain distribution along Tm_{out} and Cm_{in} for SIM 2.

Table 2 Maximum strain and deflection values and performance measures

SIM	ε_t^{max} [μm/m]	Shift t [mm]	ε_c^{max} [μm/m]	Shift c [mm]	ε_u^{max} [μm/m]	α^{max} [μm]	$K_z \times 106$ [N/m]	S_z [μm/m/N]
1	218.6	0.74	282.2	1.09	347.7	35.1	2.489	3.48
2	67.7	1.14	100.9	0.77	118.8	8.8	11.363	1.19
3	28.2	1.12	48.9	0.89	55.0	3.3	30.303	0.55
4	134.2	0.66	179.6	0.33	228.5	15.9	6.289	2.29
5	39.3	0.59	65.0	0.30	69.7	3.7	27.027	0.7
6	32.2	0.57	70.1	0.84	71.5	2.9	34.482	0.72
7	73.8	0.63	107.3	0.48	125.7	5.4	18.518	0.13
8	46.1	0.46	95.3	0.67	102.7	3.2	31.25	1.03
9	12.7	0.41	42.3	0.41	35.3	1	100	0.35

Fig. 3 shows strain, ε_u, along Tu_{in} and x-positions of the finite elements on Tu_{in} at which ε_u values are recorded, for SIM 2. The strain, ε_u, is in tensile state with positive values. The maximum value of ε_u, $\varepsilon_u^{max} = 118.8$ [μm/m], is located at the zero x-position. Table 2 lists the values of ε_u^{max} for all simulations. The shift values of ε_u^{max} are always zero.

In Table 2, it can be observed that the values of ε_u^{max} considerably larger than those of ε_t^{max} and relatively larger than the values of ε_c^{max}. As a result, it is better to employ ε_u^{max} and ε_c^{max} for the arms of any bridge used with the octal ring. This is because their large values, compared to the values of ε_t^{max}, will result in a higher sensitivity to the applied load. However, nonlinearity is unavoidable at this stage. Fig. 3, also, shows the distribution of the deflections, α, along the face Cu_{out}. The deflection is given for finite elements on Cu_{out} at different x-positions. From the figure, it can be seen that the maximum deflection, α^{max}, is 9 [μm] and is located at the zero x-position. The corresponding stiffness, K_z, is 11.363*106 N/m. The distributions of α and ε_u are similar for all simulation and α^{max} is always at zero x-position. Table 2 lists all values of α^{max} for all simulation. It also lists all calculated values of K_z and S_z for all simulations using equations 1 and 2. The S_z values listed in Table 1 are calculated based on ε_u^{max} values for $F_z = 100$ N.

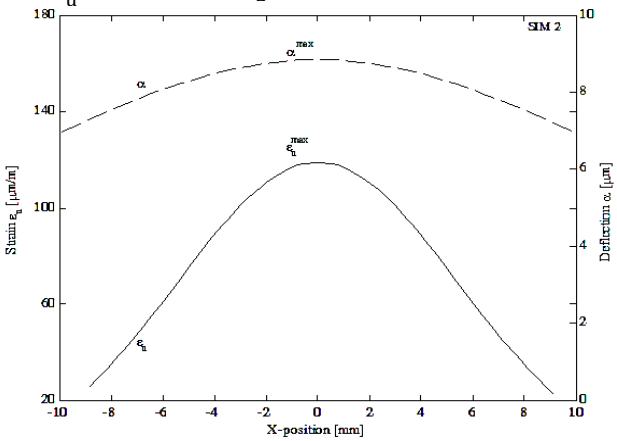

Fig. 3 Strain and deflection distributions along Tu_{in} and Cu_{out} respectively.

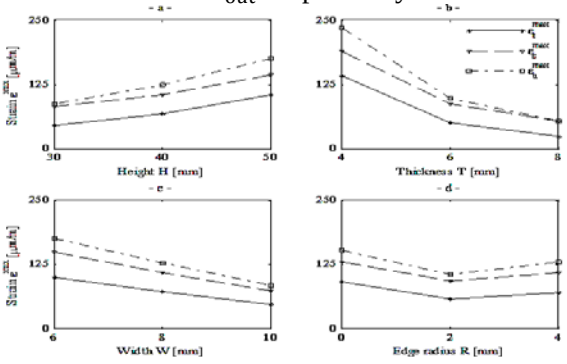

Fig. 4 Effect of different levels of design parameters on maximum strains

To analyze the effect of the different levels of the design parameters on $\varepsilon_{t,c,u}^{max}$, the graphical variation of means method has employed. The method implies calculating the average values for $\varepsilon_{t,c,u}^{max}$ for each level for each design parameter. Then, the average values have compared by plotting them as shown in Fig.4. The figure shows that increasing H increases $\varepsilon_{t,c,u}^{max}$ values while increasing T and W decreases $\varepsilon_{t,c,u}^{max}$ values. In addition, the figure shows that R does not have a direct effect on $\varepsilon_{t,c,u}^{max}$. Moreover, the figure shows that ε_{c}^{max} and ε_{u}^{max} get close to each other as T increases and as H decreases. These results are similar to the theoretical results available in the literature. In fact, the theoretical values of ε_{t}^{max} and ε_{c}^{max} were calculated for all simulation using equations 3 and 4 [6, 7]. Equation 3 is for circular rings, and strain has designated by the superscript "c" while equation 4 is for octal rings and strain has designated by the superscript "o".

$$\varepsilon_{t}^{c\ max} = \varepsilon_{c}^{c\ max} = \pm\frac{1.09\ F_z\ D}{2\ E\ W\ T^2} \qquad (3)$$

$$\varepsilon_{t}^{o\ max} = \varepsilon_{c}^{o\ max} = \pm\frac{0.7\ F_z\ D}{2\ E\ W\ T^2} \qquad (4)$$

Where E is modulus of elastically [N/mm2]

Fig. 5 compares the average values of the theoretical strains, $\varepsilon_{t,c}^{c\ max}$ and $\varepsilon_{t,c}^{o\ max}$, for each level of each design parameter as described earlier for Fig. 4.

Fig 5 also shows the values of $\varepsilon_{t}^{o\ max}$ and $\varepsilon_{t}^{o\ max}$ for the sake of comparison between simulated and theoretical strains. It is clear from the figure that the effects of the different levels of the different design parameters on $\varepsilon_{t}^{c\ max}$ and $\varepsilon_{t}^{o\ max}$ are the same as their effects on ε_{t}^{max} in terms of trends. However, simulated ε_{t}^{max} values are slightly lower than theoretical $\varepsilon_{t}^{o\ max}$ values and considerably lower than $\varepsilon_{t}^{c\ max}$ values. Fig. 5, also, shows that the averaged values of ε_{c}^{max} are located between the averaged values of $\varepsilon_{c}^{c\ max}$ and those of $\varepsilon_{c}^{o\ max}$ values.

Fig.6 shows how the different levels of the design parameters affects sensitivity. From the figure, it is possible to notice that increasing H increases S_z while increasing T and W decreases it. In addition, R does not have a direct effect on S_z.

Fig. 7 shows the effects of the different levels of the design parameters on simulated and theoretically calculated ring stiffness. Theoretical ring stiffness is given for circular and octal rings using equations 5 and 6 respectively [8].

$$k^c = \frac{4.47\ E\ W\ T^3}{R^3}[N/mm2] \qquad (5)$$

$$k^o = \frac{8\ E\ W\ T^3}{R^3}[N/mm2] \qquad (6)$$

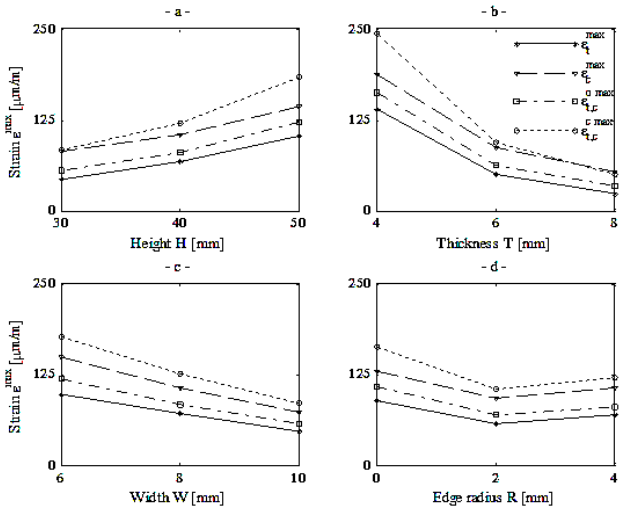

Fig. 5 Simulated and theoretical effects of design parameters on maximum strains at Tm_{out}

From the figure 7, it can be seen that increasing height, H , reduces stiffness while increasing ring thickness, T , increases stiffness considerably. The width of the ring, W , does not have clear effect of stiffness. These results are the same for simulated and theoretical results.

Fig. 4.d shows that increasing the edge radius reduces stiffness. Stiffness value is the highest for sharp edges, R = 0 [mm]. This is because edges works as obstacles to surface strain propagation from one ring face to the other. As a result, the total deflection at surface Cu_{out} is reduced.

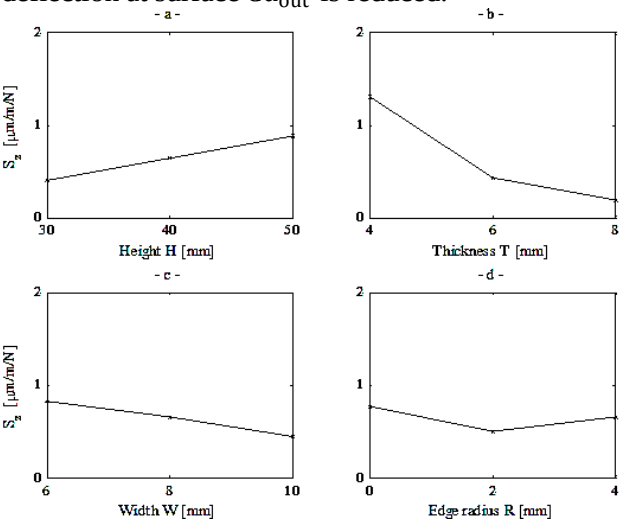

Fig. 6 Effect of design parameters on strain sensitivity S_z .

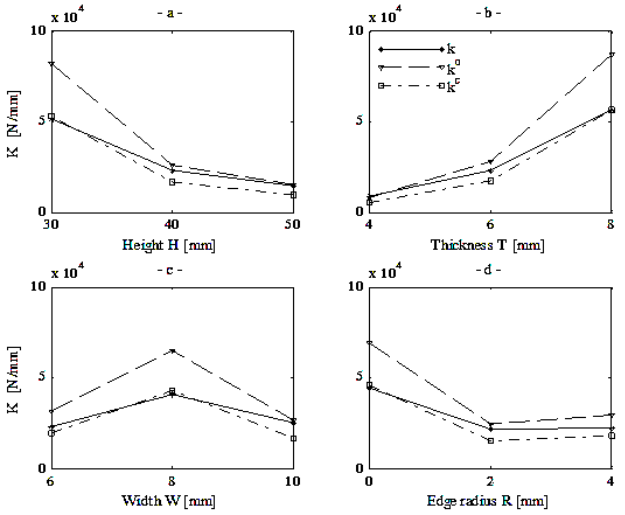

Fig. 7 Simulated and theoretical effects of design parameters on maximum strains at Cm_{in}

From Figs. 2 and 3, it is clear that ε_t^{max}, ε_c^{max} and ε_u^{max} take place at unique finite elements. As a result, they are practically difficult to measure using strain gauges. This is because a strain gauge has a finite length and therefore it measures the average strain within the region it adheres to. The average strain on Tm_{out}, ε_t^{avg}, is calculated from the equation:

$$\varepsilon_t^{avg} = \frac{1}{L_g}\int_0^{L_g} \varepsilon(z)\, dz = \frac{1}{N_s}\sum_{j=1}^{N_s} \varepsilon(j)\, E_s \qquad (7)$$

Where, L_g is the length of strain gauge and z represents the z-position of the finite element within the gauge length. The z-position is used for strain gauges at Tm_{out} and Cu_{in} while the x-position is used for strain gauge at Tu_{in}. The number of finite elements on Tm_{out} and within the length of the strain gauge, L_g, is N_s. Equation 8 gives N_s as:

$$N_s = \frac{L_g}{E_s} \qquad (8)$$

The strain gauge adheres to the strain ring so that the middle of the strain gauge is at the zero z-position for the Tm_{out} face and the Cu_{in} region and at zero x-position for the Tu_{in} face. It is evident from equation 7 that the length of strain gauge affects ε_t^{avg}, ε_c^{avg} and ε_u^{avg}.

Fig. 8 shows the effect of L_g on $\varepsilon_{t,c,u}^{avg}$ for simulations 1, 2, 4 and 7. From figure, it is clear that increasing L_g decreases $\varepsilon_{t,c,u}^{avg}$. It is also clear that there is a length of strain gauge at which ε_c^{avg} and ε_u^{avg} are equal, 17 mm for simulation 4 as an example. Such length is the optimum design length of the strain gauge for the octal ring of simulation 4. This is because such length will result in equal tensile and compressive strains in the arms of the bridge connected to the ring. As a result, the nonlinearity of the force sensor is reduced.

Fig. 9 shows the effects of F_z on $\varepsilon_{t,c,u}^{max}$ and ε_u^{avg} for SIM 2. From the figure, it is evident that ε^{max} and ε^{avg} are linearly proportional to load. The average strain ε^{avg} is given for a strain gauge length L_g = 9 [mm]. It is lower than ε_u^{max} for all load values. The figure also shows that increasing the load increases the difference between ε_u^{max} and ε_u^{avg}. This implies that the load affects stress distribution as well as the maximum strain value.

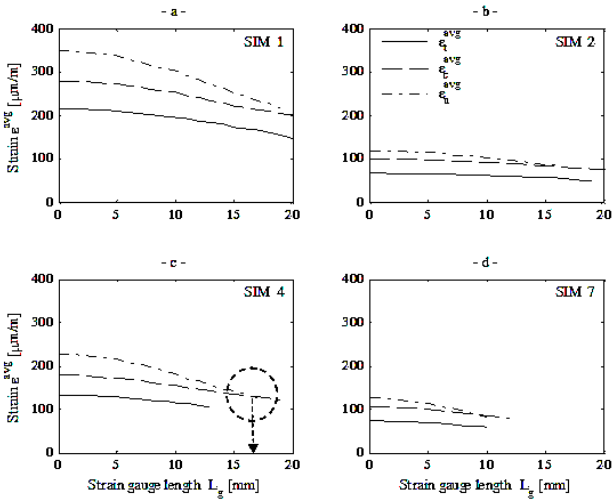

Fig. 8 Effect of gauge length on average strain.

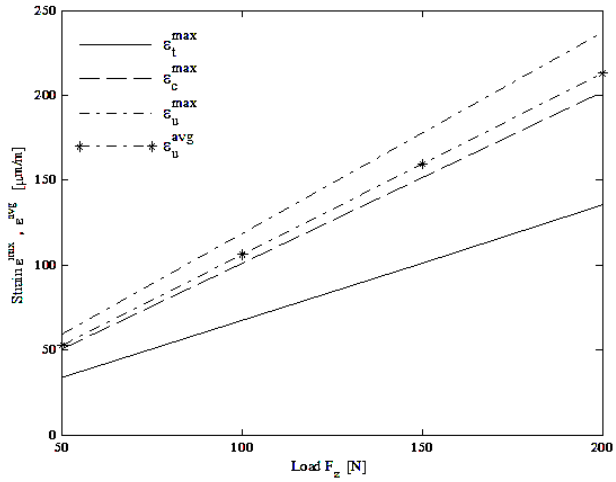

Fig. 9 Effect of load F_z on maximum strain.

5 Statistical Point of View

During statistical analysis of the interaction between the parameters (height, thickness, width, and edge curvature) to the responses (Stiffness and Sensitivity), the R-Sq of stiffness and sensitivity respectively 84.1% and 86.0% which is close to 1, indicating a high positive correlation between the parameters (height, thickness, width, and edge

curvature) to the responses (Stiffness and Sensitivity).

5.1 Regression analysis of stiffness

In this experimental study, an empirical model was developed through the regression analysis to study the parameters (height, thickness, width, and edge curvature) to the response (Stiffness). The estimated regression coefficients in the stiffness regression equation (9) shows that the following parameters; i.e., height, thickness have noteworthy influence on the stiffness. The p – value for these parameters shows that the values are approximately equal or less than alpha level of 0.05. It can therefore be concluded that there is enough statistical evidence to say that the parameters (height, thickness) influences the response (Stiffness). On the other hand, the estimated regression coefficients of width and edge curvature parameters have less influence on the stiffness. The p – value for these parameters shows that the values are higher than alpha level of 0.05. It can therefore be concluded that there is enough statistical evidence to say that the parameters (width and edge curvature) have less influence the response (Stiffness).The regression equation is

K = 35.9 - 1.76 H [mm] + 11.5 T [mm] + 0.64 W [mm]-5.14R[mm] (9)

Predictor	Coef	SE Coef	T	P
H [mm]	-1.7602	0.6671	-2.64	0.058
T [mm]	11.457	3.335	3.44	0.026
W [mm]	0.636	3.335	0.19	0.858
R [mm]	-5.139	3.335	-1.54	0.198

S = 16.3402 R-Sq = 84.1% R-Sq(adj) = 68.2%

Analysis of Variance

Source	DF	SS	MS	F	P
Regression	4	5653.2	1413.3	5.29	0.068
Residual Error	4	1068.0	267.0		
Total	8	6721.2			

Minitab software (Version 16, 2011) was used to perform the Regression Analysis of stiffness. The assumptions on which the analysis (Regression) was based upon were normality, independence, additivity, and equality of variances.

The assumptions on the Regression Analysis of Stiffness were based on were normality of residuals and homogeneity of variance for residuals. These results are indicated in Fig.10.

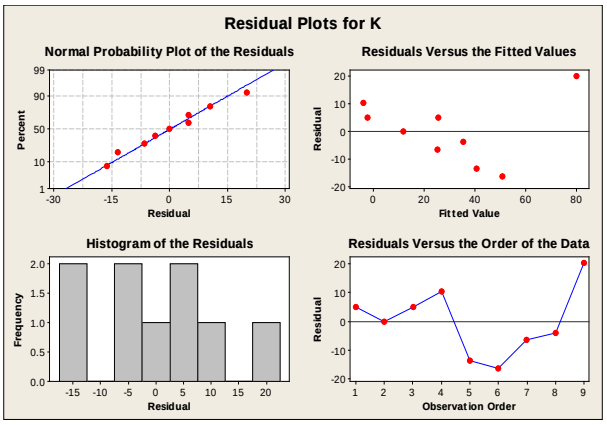

Fig. 10. The Assumptions of Analysis of Variance (Regression).

It is also clear from Fig. 11 that there is a significant difference between the parameters (height, thickness, width, and edge curvature) to the response (Stiffness). The result clearly indicates height and thickness parameters have influence on the stiffness. Moreover, the width and edge curvature parameters have less influence on the response (Stiffness).

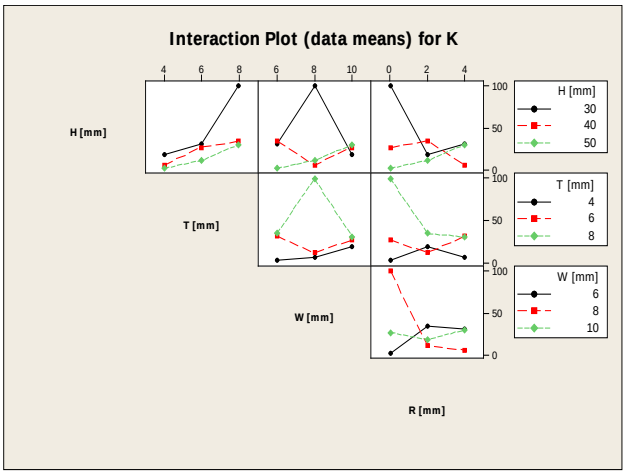

Fig. 11. Interaction plot for the parameters (height, thickness, width, and edge curvature) to the response (Stiffness).

5.2 Regression analysis of sensitivity

In this experimental study, an empirical model was developed through the regression analysis to study the parameters (height, thickness, width, and edge curvature) to the response (Sensitivity). The estimated regression coefficients in the sensitivity regression equation (10) shows that the following parameters; i.e., height, thickness, width have noteworthy influence on the sensitivity. The p – value for these parameters shows that the values are approximately equal or less than alpha level of 0.05.

It can therefore be concluded that there is enough statistical evidence to say that the parameters (height, thickness, width) influences the response (Sensitivity). On the other hand, the estimated regression coefficient of edge curvature parameter has less influence on the sensitivity. The p – value for this parameter shows that the value is higher than alpha level of 0.05. It can therefore be concluded that there is enough statistical evidence to say that the parameter (edge curvature) has less influence the response (Sensitivity). The regression equation is:

S = 3.50 + 0.0618 H [mm] - 0.357 T [mm] - 0.321 W [mm] - 0.055 R [mm] (10)

Predictor	Coef	SE Coef	T	P
Constant	3.503	1.509	2.32	0.081
H [mm]	0.06183	0.02311	2.68	0.055
T [mm]	-0.3567	0.1155	-3.09	0.037
W [mm]	-0.3208	0.1155	-2.78	0.050
R [mm]	-0.0550	0.1155	-0.48	0.659

S = 0.565973 R-Sq = 86.0% R-Sq(adj) = 72.1%

Analysis of Variance

Source	DF	SS	MS	F	P
Regression	4	7.8901	1.9725	6.16	0.053
Residual Error	4	1.2813	0.3203		
Total	8	9.1714			

Minitab software (Version 16, 2011) was used to perform the Regression Analysis of sensitivity. The assumptions on which the analysis (Regression) was based upon were normality, independence, additivity, and equality of variances. The assumptions on the Regression Analysis of Sensitivity were based on were normality of residuals and homogeneity of variance for residuals. These results are indicated in Fig. 12.

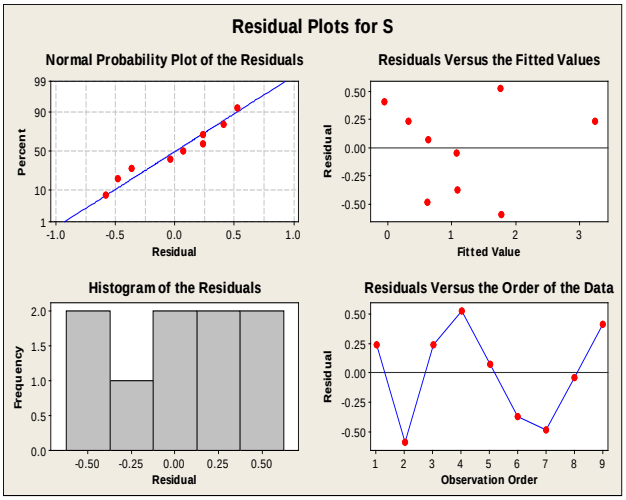

Fig. 12. The Assumptions of Analysis of Variance (Regression).

It is also clear from Fig. 13 that there is a significant difference between the parameters (height, thickness, width, and edge curvature) to the response (Sensitivity). The result clearly indicates the height, the thickness, and the width parameters have influence on the sensitivity. Moreover, the edge curvature parameter has less influence on the response (Sensitivity).

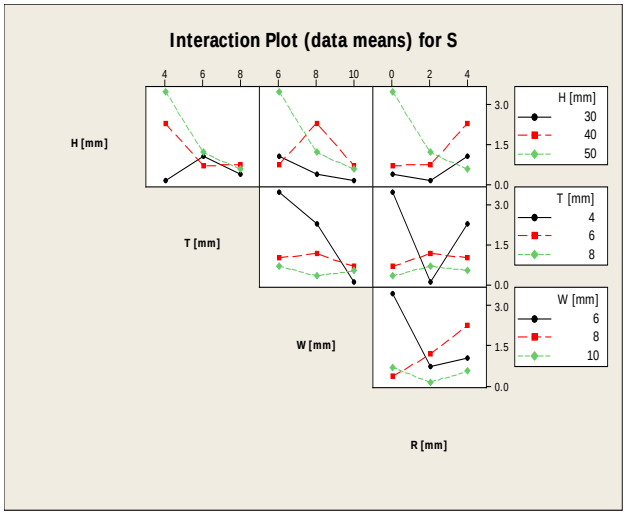

Fig. 13. Interaction plot for the parameters (height, thickness, width, and edge curvature) to the response (Sensitivity).

6 Conclusions

Based on research findings, we can conclude that the regressions models for calculation of the parameters (height, thickness, width, and edge curvature) to the responses (Stiffness and Sensitivity) are developed.

The R-Sq of stiffness and sensitivity respectively 84.1% and 86.0% which is close to 1, indicating a high positive correlation between the parameters (height, thickness, width, and edge curvature) to the responses (Stiffness and Sensitivity).

Among different interactions, interactions between thickness parameter and responses (Stiffness and Sensitivity) are most significant. Simulations showed that considerable variation in strain along ring face.

The relation between strain gauge length and strain showed that an optimal gauge length improves ring performance.

Simulation results showed that maximum compressive strain is considerably larger than maximum tensile strain. They also revealed a region of large tensile strain within the ring not exploited in the literature.

Acknowledgments

Financial and in-kind received support from the Deanship of Scientific Research, Vice Rectorate for Post Graduate and Scientific Research, Prince Sattam bin Abduaziz University (PSAU) is gratefully acknowledged. Financial support of this work through the Deanship of scientific research, Prince Sattam Abdul Aziz University, under project # 2001/01/2014 is gratefully acknowledged.

References:

[1] M. Korencke, M.L. Hull, 1989. A method for designing multi-load component dynamometers incorporating octagonal strain rings. *Journal of experimental mechanics*. June, 195-204.

[2] Jeong – Du Kim, Dang-SikKim, 1997. Development of a combined-type tool dynamometer with a piezo-film accelerometer for an ultra-precision lathe. *Journal of Materials Processing Technology*. 71, 360-366.

[3] Ulvi Seker, Abdullah Kurt, Ibrahim Ciftci, 2002. Design and construction of a dynamometer for measurement of cutting forces during machining with linear motion. *Journal of Materials and Design*. 23, 355–360.

[4] Ihsan Korkot, 2003. A dynamometer design and its construction for milling operation. *Journal of Materials and Design*. 24, 631-637.

[5] Sedat Karabay, 2007. Analysis of drill dynamometer with octagonal ring type transducers for monitoring of cutting forces in drilling and allied process. *Journal of Materials and Design*. 28, 673-685.

[6] SuleymanYaldiz, FarukUnsacar, 2006. Design, development and testing of a turning dynamometer for cutting force measurement. *Journal of Materials and Design*. 27, 839–846.

[7] SuleymanYaldiz, FarukUnsacar, 2006. A dynamometer design for measurement the cutting forces on turning. *Journal of Measurement*. 39, 80–89.

[8] Y. Chen, N.B. McLaughlin, S. Tessier, 2007. Double extended octagonal ring (DEOR) drawbar dynamometer. *Journal of Soil & Tillage Research*. 93, 462–471.

[9] Sadat Karabay, 2007. Analysis of drill dynamometer with octagonal ring type transducers for monitoring of cutting forces in drilling and allied process. *Journal of Materials and Design*. 28, 673–685.

[10] Sadat Karabay“Design, 2007. Criteria for electro-mechanical transducers and arrangement for measurement of strains due to metal cutting forces acting on dynamometers. *Journal of Materials and Design*. 28, 496–506.

[11] Sadat Karabay, 2007. Performance testing of a constructed drilling dynamometer by deriving empirical equations for drill torque and thrust on SAE 1020 steel. *Journal of Materials and Design*. 28, 1780–1793.

[12] SuleymanYaldiz, FarukUnsacar, Haci Saglam, Hakan Isik, 2007. Design, development and testing of a four-component milling dynamometer for the measurement of cutting force and torque. *Journal of Mechanical System and Signal Processing*. 21, 1499–1511.